STRESS TRANSFER IN CARBON NANOTUBE REINFORCED POLYMER COMPOSITES

A. Haque and A. Ramasetty

Department of Aerospace Engineering and Mechanics, The University of Alabama, Tuscaloosa, AL – 35487, USA

ABSTRACT

An analytical model has been developed to study stress transfer in single walled carbon nanotube (SWNT) reinforced polymer matrix composites. The model predicts axial stress and interfacial shear stress distribution along the carbon nanotube (CNT) embedded in matrix materials. A simplified representative volume element (RVE) has been considered in the analysis. The model is based on an existing improved two-dimensional stress transfer model for platelet reinforced composites. An expression for the effective length of the carbon nanotube (CNT) has also been derived for efficient load transfer in CNT reinforced composites. The effects of CNT aspect ratio, CNT volume fraction and matrix modulus on stress transfer has been analyzed in details. Finally, the results from the analytical model are compared with finite element analysis.

1. INTRODUCTION

The exceptional mechanical, thermal and electrical properties of carbon nanotubes (CNTs) show significant promises as a potential reinforcing phase in polymer matrix composites [1-3]. The mechanical behavior of carbon nanotube reinforced polymer composites (CNPC) depends on the load transfer efficiency between the CNT and the surrounding matrix materials. The subject of load transfer in conventional short fiber reinforced composites has been studied using shear lag models for many decades. Cox [4] proposed a shear lag model for a single fiber embedded in matrix subjected to uniform displacement in the fiber direction. It was assumed that the rate of stress transfer from the matrix to fiber is proportional to the difference between the axial displacement at a point in the fiber and the corresponding displacement at the same point in the matrix without the fiber present. To obtain an analytical solution, he further assumed that the axial displacement at the outer circumference of the matrix is not effected by the fiber. Hsueh [5] developed a two-dimensional stress transfer model for platelet reinforcement. Unlike Cox's model, the uniform stress was applied on the loading surface of the unit cell. Hsueh assumed that the shear stress in the matrix decreases linearly from the interface between the platelet and matrix to the edges. Both bonded and disbonded end cases of the platelet were considered in his analysis. Fu et al [6] investigated the influence of neighboring unidirectional multi-short-fiber on the stress transfer by including the effects of the composite medium. The fiber distribution was assumed to be uniform in the composite and the effects of fiber aspect ratio, fiber volume fraction, fiber end gap and fiber-matrix modulus ratio on the stress transfer were studied. The load transfer efficiency in the platelet reinforced nanoclay composites and the effect of platelet dispersion have also been investigated by Tsai and Sun [7]. To our knowledge no studies are reported on predicting stress transfer of CNT reinforced composites. In this paper, the model that Hsueh [5] and Tsai [7] applied to platelet reinforced composite is extended to CNPC. The micromechanical model presented in this paper is capable of predicting the effective length, L_{eff}, the axial stress, σ_n and shear stress, τ_i of the SWNT/matrix interface. The results from analytical model are compared with finite element analysis.

2. STRESS TRANSFER AT NANOTUBE INTERFACE

Analytical Model

Carbon nanotube reinforced polymer composite (CNPC) with uniformly distributed single walled carbon nanotube (SWNT) is shown in Fig. 1(a). Considering the periodicity, a representative volume element (RVE) used in the load transfer analysis is shown in Fig. 1(b). We have neglected the effects of end gap in our analysis due to high aspect ratio of the carbon nanotube. Applying proper boundary conditions, the RVE can be used to obtain expression for axial stress, interfacial shear stress and the load transfer efficiency at the CNT matrix interface. Fig. 2 shows a 2D unit cell model of carbon nanotube reinforced composites under a uniform applied tensile load σ_o without end bonding. A carbon nanotube with a length 2L, inner and outer radii, R_i and R_o is embedded at center of the matrix materials with a width 2b as shown in Figure 2. In this analysis, we have first derived the governing equation for the stress transfer between the nanotube and the matrix. Second, the general solution of the stress distribution is derived. Finally, expression for the effective length of the load transfer efficiency is provided.

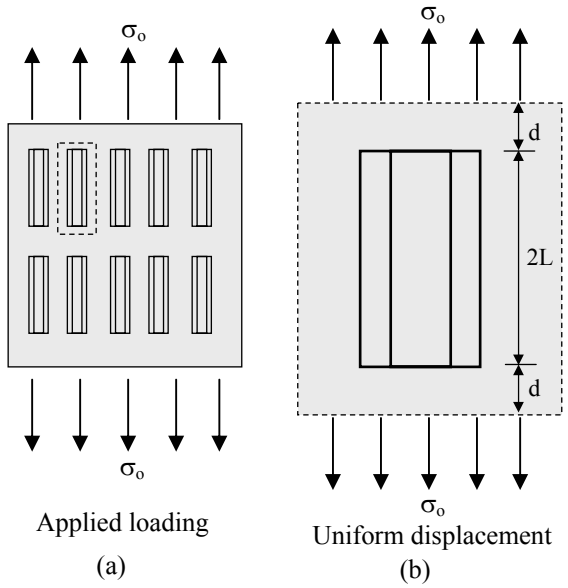

Fig. 1 Carbon Nanotube composite: (a) Uniformly distributed SWNT (b) RVE

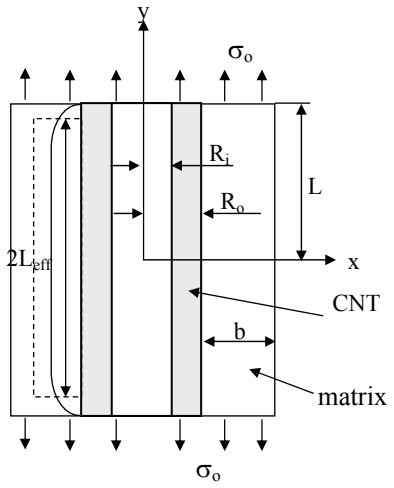

Fig. 2 2D unit cell model without end bonding

Stress Transfer Equation

The equilibrium equation between the normal stress, σ_y, and the shear stress, τ_{xy} for two-dimensional geometry, is [8]

$$\frac{\partial \sigma_y}{\partial y} + \frac{\partial \tau}{\partial x} = 0 \qquad \text{-- (1)}$$

Applying the force equilibrium equation in 'y' direction for a differential length of the CNT from the RVE, we can have the following differential equation relating the rate of change of nanotube normal stress, σ_n along the y axis and the interfacial shear stress, τ_i.

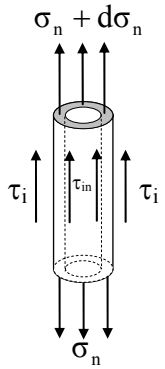

Fig. 3

$$\left[\frac{\pi}{4}(d_o^2 - d_i^2)\right](\sigma_n + d\sigma_n) - \left[\frac{\pi}{4}(d_o^2 - d_i^2)\right]\sigma_n + \pi d_o \tau_i dy + \pi d_i \tau_{in} dy = 0 \text{ --- (2)}$$

$$\frac{d\sigma_n}{dy} = -2\left[\frac{R_o\tau_i + R_i\tau_{in}}{R_o^2 - R_i^2}\right] \quad \text{-- (3)}$$

Assuming, $\tau_{in} = \tau_i$ for nanoscale thickness of the cylinder

$$\frac{d\sigma_n}{dy} = -\frac{2\tau_i}{R_o - R_i} \quad \text{-- (4)}$$

Stress Distribution in Nanotube

According to classical shear lag model for the cylindrical geometry, the stress variation is considered only in the loading direction (axial 'y' direction) and ignored in the direction normal to it ('x' direction) [4**].** Based on this assumption, the gradient of the normal stress, σ_y in the y direction in the matrix can be approximated by a function, f(y) **[**5**],** where $\sigma_{y=}\sigma_m$

$$\frac{\partial\sigma_m}{\partial y} = f(y) \quad \text{-- (5)}$$

Applying Eq. 5. in the equilibrium Eq. 1., we get

$$\frac{\partial\tau}{\partial x} = -f(y) \quad \text{-- (6)}$$

Solution of Eq. 6. for two boundaries, $x = R_o$ and $R_o \le x < (b + R_o)$, provides interfacial shear stress, τ_i, and shear stress, τ_m as x-dependence in matrix materials

$$\tau_m = (b + R_o - x)\, f(y), \quad \text{for } (R_o \le x < (b + R_o) \text{ -- (8)}$$

$$\tau_i = b\,.\,f(y), \quad \text{for } x = R_o,\ \tau = \tau_i \text{ -- (9)}$$

Eliminating f(y) from Eqs. 8. & 9., we get a relationship between τ_m and τ_i

$$\tau_m = \frac{(b + R_o - x)}{b}\tau_i \quad \text{-- (10)}$$

Again, from stress displacement relationship while load being applied in y direction, τ_m can be approximated to displacement, v_m in the y direction by

$$\tau_m = \frac{E_m}{2(1+\upsilon_m)}\frac{dv_m}{dx} \quad \text{-- (11)}$$

where, E_m and υ_m are the Young's modulus and Poisson's ratio of the matrix, respectively

Now, equating Eq. 10. and 11. and integrating both side from R_o to $R_o + b$, we can have τ_i in terms of displacement v_{R_o+b} at $x = R_o + b$ and v_{R_o} at $x = R_o$

$$\tau_i = \frac{E_m}{b(1+\upsilon_m)}(v_{R_o+b} - v_{R_o}) \quad (12)$$

Substituting Eq. 12. in Eq. 10., we also get expression of τ_m in terms of displacement v_{R_o+b} at x = R_o + b and v_{R_o} at x = R_o

$$\tau_m = \frac{(b + R_o - x)}{b^2(1+\upsilon_m)}(v_{R_o+b} - v_{R_o})\, E_m \tag{13}$$

Now from Eq. 11. and 13., the displacement v_m can be derived

$$v_m = v_{R_o} + \frac{\left[-2bR_o - R_o^2 + 2(b+R_o)x - x^2\right]}{b^2}(v_{R_o+b} - v_{R_o}) \tag{14}$$

Differentiation of Eq. 14. with respect with 'y' & then multiplication with E_m provides

$$\sigma_m = \sigma_{R_o} + \frac{\left[-2bR_o - R_o^2 + 2(b+R_o)x - x^2\right]}{b^2}(\sigma_{R_o+b} - \sigma_{R_o}) \tag{15}$$

where, σ_m is the axial stress in the matrix, $\sigma_m = \sigma_{Ro}$ at x = R_o and $\sigma_m = \sigma_{Ro+b}$ at x = R_o +b

The mechanical equilibrium condition between applied stress σ_o and the stress distribution in the composite require that

$$(R_o - R_i)\sigma_n + \int_{R_o}^{b+R_o} \sigma_m dx = (b + R_o - R_i)\sigma_o \tag{16}$$

From Eq. 15. and 16.

$$\sigma_{Ro+b} = \sigma_{R_o} + \frac{3}{2b}\left[(b + R_o - R_i)\,\sigma_o - (R_o - R_i)\sigma_n - b\,\sigma_{R_o}\right] \tag{17}$$

Combining Eq. 4., 12. and 17.

$$\frac{d^2\sigma_n}{dy^2} = \frac{3\left[b\,\sigma_{R_o} + (R_o - R_i)\sigma_n - (b + R_o - R_i)\,\sigma_o\right]}{(1+\upsilon_m)b^2(R_o - R_i)} \tag{18}$$

For perfect bonding,

$$\sigma_{R_o} = \frac{E_m}{E_n}\sigma_n \tag{19}$$

From Eq. 18. & 19.

$$\frac{d^2\sigma_n}{dy^2} = \frac{3\left[b\,E_m + (R_o - R_i)E_n\right]}{(1+\upsilon_m)b^2(R_o - R_i)E_n}\,\sigma_n - \frac{3(b + R_o - R_i)}{(1+\upsilon_m)b^2(R_o - R_i)}\sigma_o \tag{20}$$

From Eqs. (20) and (4) we get

$$\sigma_n = \frac{(b + R_o - R_i)E_n\sigma_o}{(R_o - R_i)E_n + bE_m} + Ae^{\alpha y} + Be^{-\alpha y} \tag{21}$$

$$\tau_i = -\frac{\alpha(R_o - R_i)}{2}\left[Ae^{\alpha y} - Be^{-\alpha y}\right] \tag{22}$$

where

$$\alpha = \frac{1}{b}\left\{\frac{6\left[(R_o - R_i)E_n + bE_m\right]G_m}{(R_o - R_i)\,E_n.E_m}\right\}^{1/2},$$

E_n and E_m are the moduli of elasticity of the SWNT and matrix. Coefficients A and B can be determined using the two boundary conditions, $\sigma_n = \sigma_o$ at y = L and $\tau_i = 0$ at y = 0. Substituting coefficients A and B in Eqs. (21) and (22), we get

$$\sigma_n = \frac{(b + R_o - R_i)\, E_n \sigma_o}{(R_o - R_i)\, E_n + bE_m} + \frac{e^{\alpha y} + e^{-\alpha y}}{e^{\alpha L} + e^{-\alpha L}} \left[1 - \frac{(b + R_o - R_i) E_n}{(R_o - R_i) E_n + bE_m} \right] \sigma_o \tag{23}$$

$$\tau_i = \frac{(R_o - R_i)\, \alpha}{2} \left[\frac{b\,(E_m - E_n)}{(R_o - R_i) E_n + bE_m} \right] \frac{e^{\alpha y} + e^{-\alpha y}}{e^{\alpha L} + e^{-\alpha L}} \sigma_o \tag{24}$$

Effective Length

In the case of long SWNT in the matrix, the axial stress in the fiber increases from both ends under uniaxial loading and reaches to a saturated point at some fiber length. To achieve most of the saturation stress along the length of the nanotube the load transfer should be maximized. The effective length, L_{eff} is defined to determine the efficiency of the load transfer from the matrix to the carbon nanotube. The effective length, L_{eff} of the SWNT is the length in which the equivalent amount of the saturated load is carried and mathematically defined as follows:

$$\sigma_n^s\, L_{eff} = \frac{1}{2} \int_{-L}^{L} \sigma_n \, dy \tag{25}$$

where σ_n is axial stress and σ_n^s is saturated stress in the SWNT.

Now, saturated stress, σ_n^s can be determined by letting L to infinity in eqn (25)

$$\sigma_n^s = \frac{(b + R_o - R_i)\, E_n \sigma_o}{(R_o - R_i)\, E_n + bE_m} \tag{26}$$

Substituting σ_n & σ_n^s into Eq. 26., we finally get the expression of effective length, L_{eff} for SWNT as follows:

$$L_{eff} = L + \tanh(\alpha L) \frac{\left[1 - \frac{(b + R_o - R_i)\, E_n \sigma_o}{(R_o - R_i)\, E_n + bE_m} \right]}{\alpha \left[\frac{(b + R_o - R_i)\, E_n \sigma_o}{(R_o - R_i)\, E_n + bE_m} \right]} \tag{27}$$

Finite element analysis

The finite element analysis of the CNT reinforced polymer matrix was done using a quarter symmetric model. Eight nodded hybrid solid element (C3D8I) was used in the analysis [9]. This solid element has extra incompatible deformation modes in addition to the displacement degrees of freedom. These degrees of freedom eliminate the parasitic shear stresses that are observed in regular displacement elements if there are loaded in bending. Table 1 shows the properties of the SWNT and the matrix that were used in the analysis. The quarter symmetric geometric model of the CNPC is shown in Fig. 4. Finite element analysis was carried out for various aspect ratios of SWNT. Loading conditions applied in the model was similar to that considered in the analytical study. Fig. 5 shows the boundary conditions and the applied load in the present study. In this

study, one end of the CNPC was fixed and a pressure load was applied at the other end. The stress distribution at the interface of the matrix and the SWNT was investigated. The results obtained in FEA study were compared with the analytical results.

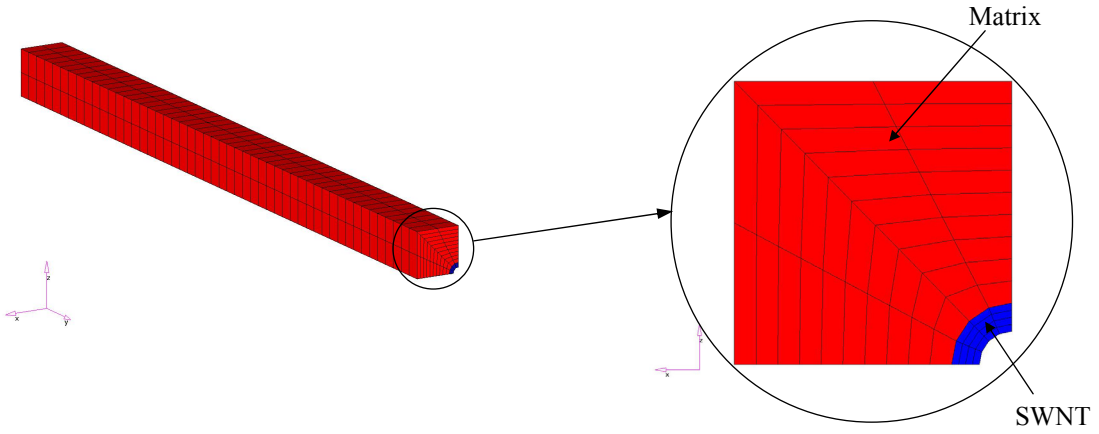

Fig. 4 Quarter symmetric FEA model of CNPC

Table 1 Properties of SWNT and matrix used in finite element analysis

Property	SWNT	Matrix
Modulus of elasticity, E (Pa)	1×10^{12}	3.75×10^{8}
Poisson's ratio, υ	0.35	0.30
Type of element	Solid	Solid

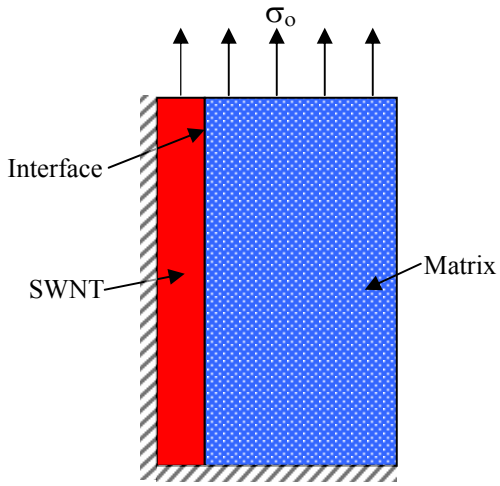

Fig. 5 Geometric Model with Boundary Conditions & Applied Load

3. RESULTS AND DISCUSSION

Effects of CNT aspect ratios (l/d)

Figure 6 show effects of CNT aspect ratios (l/d – 10 to 1000) on axial stress transfer along the CNT length. The results from both analytical and finite element analysis (FEA) are compared in this study. The trends of the stress transfer plots are observed to be similar in both the cases. The results show approximately zero stress at the CNT ends indicating almost no stress transfer. The stress level increases gradually from the CNT ends and then gradually it reaches to a saturation stage at the CNT center point. Such saturation points are particularly observed at CNT aspect ratio above 10. The rate at which axial stress increases and also the length of the saturation plateau along the CNT length are shown to be higher for increased CNT aspect ratios. It is clearly evident from Fig. 6 that the axial stress transfer mostly occurs through CNT length and the

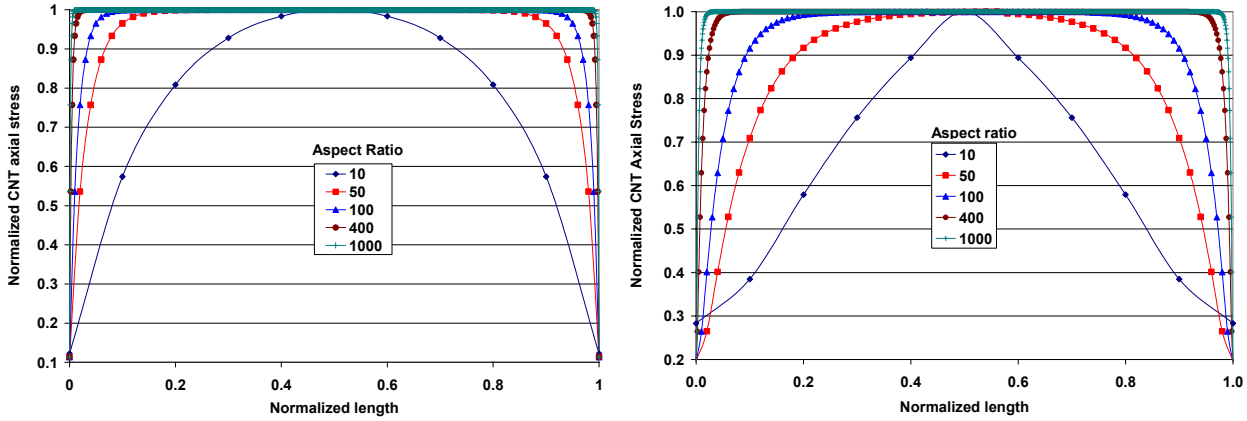

(a) **(b)**

Fig. 6 Normalized CNT axial stress vs. normalized CNT length **(a)** analytical model **(b)** finite element analysis

length of the saturation plateau covers almost the entire CNT length at aspect ratio above 1000. A symmetric stress distribution is also observed about the mid-section of the CNT. The result from analytical method shows comparatively higher axial stress transfer than that obtained from FEA. A reasonable agreement is observed between the analytical and FEA model.

Figure 7 shows the plots of normalized interfacial shear stress vs. normalized CNT length for various CNT aspect ratios. The interfacial shear stress distribution predicted from both analytical method and finite element analysis are presented in Figure 7. The results show maximum interfacial shear stress at the CNT ends which gradually decreases to zero at the CNT center point particularly for aspect ratios(l/d) above 50. Such trend is completely reverse in the case of CNT axial stress transfer as shown in Fig. 6. The rate at which the interlaminar shear stress decreases along the CNT length is observed to be higher in the analytical model as compared to finite element analysis. In both the cases the plateau length with zero interlaminar shear stress is observed to be larger with increased CNT aspect ratios. At aspect ratio above 1000 the length of

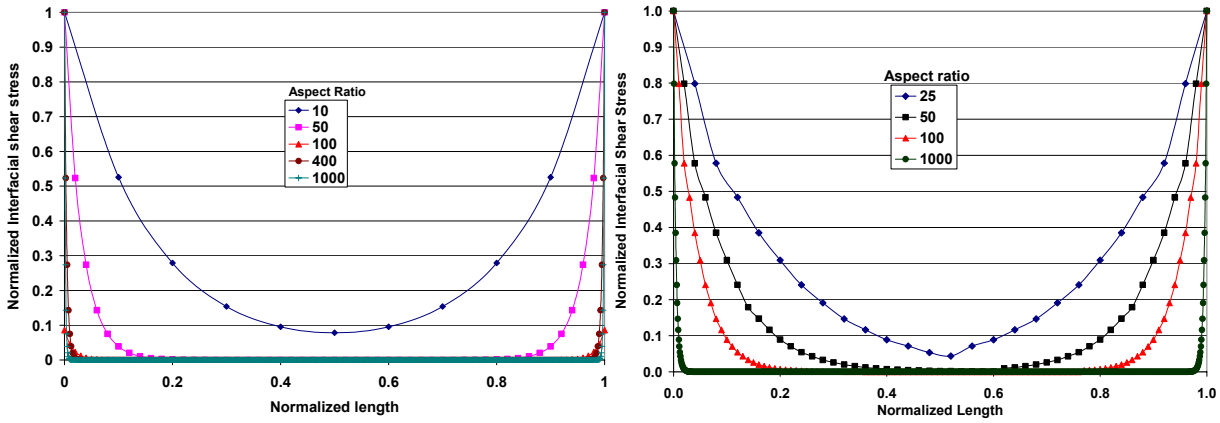

(a) **(b)**

Fig. 7 Normalized interfacial shear stress vs. normalized CNT length **(a)** analytical method (b) finite element analysis

such plateau reaches to an optimum value covering almost the entire CNT length. The analytical model and finite element analysis show reasonable agreement between interlaminar shear stress transfer for various aspect ratios.

Effects of CNT Volume Fraction (V_{cnt})

Figure. 8 shows the effects of CNT volume fractions (4 % to 10 %) on axial stress and interfacial shear stress distribution along the normalized CNT length. It is to be noted that in most of CNT reinforced composites the volume fractions of the reinforcing phase are limited to maximum 10 % due to dispersion problems. The data points in these plots are determined using the analytical model. An aspect ratio of 200 was selected for this study. At this aspect ratio the plateau length was almost close to optimum CNT length. The results show slightly enhanced axial stress and reduced interfacial shear stress with increased CNT volume fractions. The trends of the plots were almost similar as observed in earlier cases.

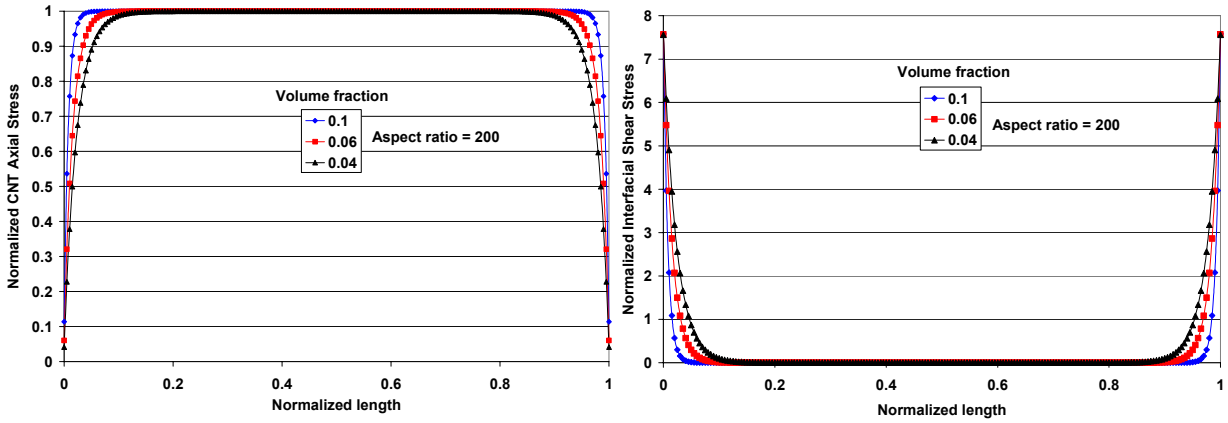

Fig. 8 Effects of volume fraction on axial stress and interfacial shear stress along the CNT length

Effects of Matrix Modulus

Figure 9 show the effects of matrix modulus on axial stress and interfacial shear stress distribution along the CNT length. There is no noticeable change in both the CNT axial stresses as well as the interfacial shear stresses when the modulus of the matrix increased by 3 times and reduced by 90%. So, we can assume that matrix material has a very little effect on the CNT axial stresses and the interfacial shear stresses. This is possibly due to the fact that the modulus of the carbon nanotube is significantly high compared the modulus of the matrix materials.

Load Transfer Efficiency

Table 2 provides the comparison of L_{eff} and L_{eff}/L at various aspect ratios (10- 5000) determined by analytical model and finite element analysis. Figure 10 shows plots of such data points L_{eff}/L vs. aspect ratios(l/d). In both the cases L_{eff}/L increases with increased aspect ratios. But such increases are significantly higher at lower aspect ratios. At very low aspect ratio (100), the differences in magnitude of L_{eff}/L between FEA and analytical model was approximately 80%.

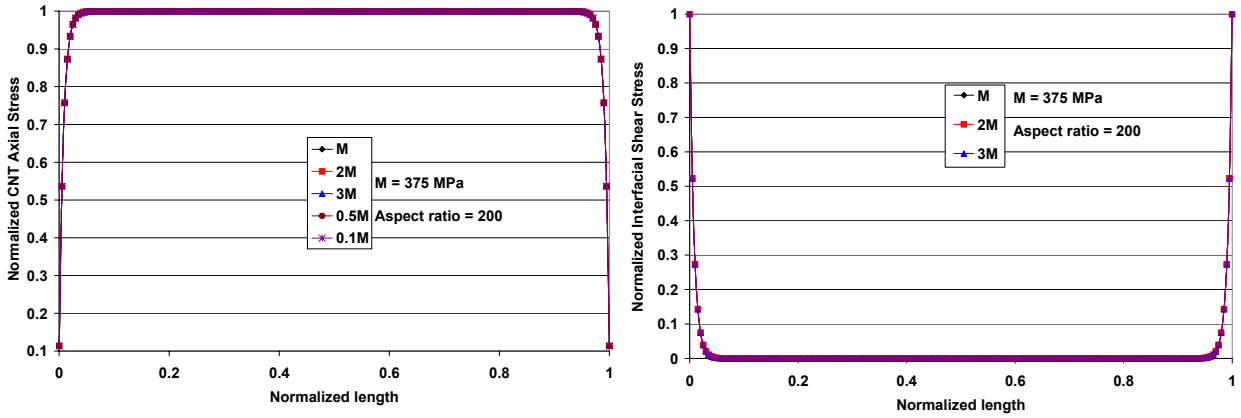

Fig. 9 Effects of matrix modulus on CNT axial stress and interfacial shear stress

These differences are observed to be significantly less at higher aspect ratios (1000-5000). Moreover, in all the cases the magnitude of L_{eff}/L determined by the analytical model was comparatively higher than the result obtained from FEA study. Both the FEA and analytical model almost converges at aspect ratio, L/d = 5000.

Table 2 Comparison of L, L_{eff} and L_{eff}/L at various aspect ratios for finite element model and analytical model

Aspect ratio, 2L/d	L (nm)	Finite Element Model		Analytical Model	
		L_{eff} (nm)	L_{eff}/L	L_{eff} (nm)	L_{eff}/L
10.00	5.00	-	-	3.46	0.6779
50.00	25.00	-	-	23.46	0.9356
100.00	50.00	17.00	0.3400	48.46	0.9678
150.00	75.00	42.00	0.5600	73.46	0.9785
200.00	100.00	67.00	0.6700	98.46	0.9839
400.00	200.00	167.00	0.8350	198.46	0.9919
1000.00	500.00	467.00	0.9340	498.46	0.9968
1500.00	750.00	717.00	0.9560	748.46	0.9979
2000.00	1000.00	967.00	0.9670	998.46	0.9984
3000.00	1500.00	1467.00	0.9780	1498.46	0.9989
4000.00	2000.00	1967.00	0.9835	1998.46	0.9992
5000.00	2500.00	2467.00	0.9868	2498.46	0.9994

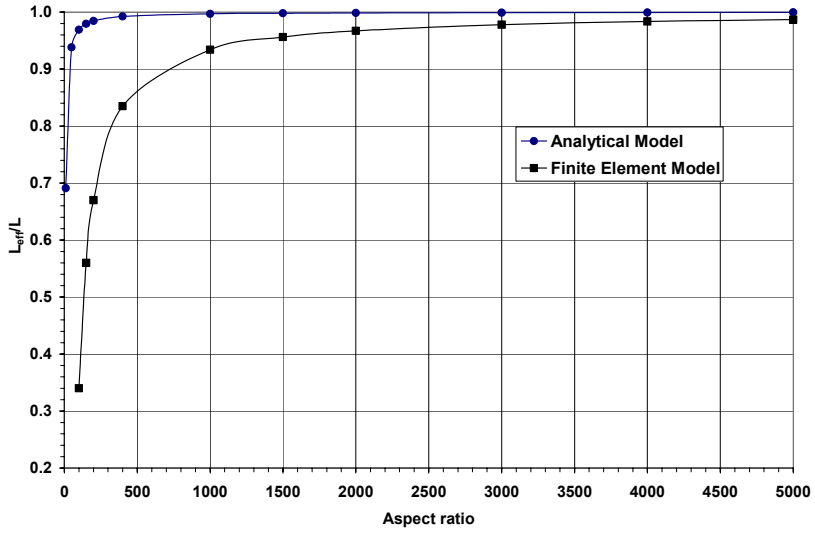

Fig. 10 Load transfer efficiency (L_{eff}/L) as a function of aspect ratio (L/D)

4. CONCLUSIONS

An analytical model has been developed to investigate the load transfer efficiency of carbon nanotube (CNT) reinforced polymer matrix composites. Finite element analysis (FEA) has also been carried out in parallel to validate the results generated from the analytical model. The effects of aspect ratio, fiber volume fractions and matrix modulus on the axial stress and interfacial shear stress along the CNT length has been studied. The axial stress reached to a saturation point at the CNT center for CNT aspect ratio above 10 and diminished toward zero at the ends. In contrary, the interfacial shear stress showed maximum at the CNT ends and falls to zero in the center. An optimum CNT aspect ratio is observed to be approximately 1000 for efficient load transfer in CNT reinforced polymer nanocomposites. The results show insignificant increase in axial stress and decrease in interfacial shear stress due to enhanced of CNT volume fraction (4 % to 10 %). The results show reasonable agreement between the results obtained from analytical model and finite element analysis particularly at higher aspect ratio.

References

1. **Iijima, S.**, "Helical microtubules of graphitic carbon", *Nature* **354** (1991), 56-58.
2. **Lu, J. P.**, "Elastic Properties of Single and Multilayered Nanotubes", *Journal of Physics and Chemistry of Solids*, **58**/11 (1997), 1649-1652.
3. **Thostenson, E. T., Ren, Z.** and **Chou, T. W.**, "Advanced in the Science and Technology of Carbon nanotubes and their Composites: A Review", *Composites Science and Technology*, **61**/13 (2001), 1899-1912.
4. **Cox, H. L.,** "The Elasticity and Strength of Paper and Other Fibrous Materials", *British Journal of Applied Physics*, **3** (1952), 72-79.
5. **Hsueh, C.,** "A Two-dimensional Stress Transfer Model for Platelet Reinforcement", *Composites Engineering*, **4**/10 (1994), 1033-1043.
6. **Fu, S. Y., Yue, C. Y., Hu, X.** and **Mai, Y. W**, "On the Elastic Transfer and Longitudinal Modulus of Unidirectional Multi-Short Fiber Composites", *Com. Sci. Tech.*, **60** (2000), 3001-3012.
7. **Tsai, J.** and **Sun, C. T.** "The Effect of Platelet Dispersion on the Load Transfer Efficiency in Nanoclay Composites", *Proceedings of The American Society for Composites* (2002).
8. **Timoshenko, S. P.** and **Goodier, J. N.,** "Theory of Elasticity", Third edition, McGraw-Hill International Editions.
9. ABAQUS user manual.